Simultaneous Surface Segmentation and BRDF Estimation via Bayesian Methods

Malte Lenoch, Thorsten Wilhelm and Christian Wöhler
Image Analysis Group, TU Dortmund University, Otto-Hahn-Strasse 4, Dortmund, Germany

Keywords: Image Segmentation, BRDF Estimation, Reversible Jump Markov Chain Monte Carlo.

Abstract: We present a novel procedure that achieves segmentation of an arbitrary surface relying on the maximum a-posteriori estimation of its reflectance parameters. The number of surfaces segments is computed by the algorithm without user intervention. We employ Markov Chain Monte Carlo algorithms to compute the probability distributions associated with the model parameters of a Blinn reflectance model based on the input images. The fact that parameters are treated as probability distributions enables us to directly draw additional information about the certainty of the estimation from the results of both parameters and segmentation borders. Reversible jump MCMC allows us to include an unspecified number of change points in the computation, such that the algorithm explores model and parameter space at the same time and derives a segmentation of the surface from the input data. To accomplish this, we extend the existing concept of change points to two dimensions introducing a number of necessary new regulations and properties. The performance of the segmentation and reflectance estimation is evaluated on a synthetic and a real-world dataset.

1 INTRODUCTION

Many man-made objects or natural materials exhibit a reflectance that is non-uniform across the surface. The estimation of a spatially varying bi-directional reflectance distribution function (SVBRDF) is a well-approached research task in computer vision as well as in photogrammetric backgrounds. Additionally, it is of interest in certain tasks, to determine the surface areas that consist of the same material and are therefore associated with identical reflectance properties.

Our goal is to segment the surface of an arbitrary object into meaningful regions based on the reflection properties of those particular regions. We apply methods from Bayesian statistics to compute the posterior of the acquired BRDF parameters and the patch borders based on the given input data and the specified prior distributions, reflecting knowledge which is at hand prior to the experiment. Since we handle every parameter as a stochastic distribution, we know the uncertainty of the estimate as well, instead of only handling a point estimate as do common gradient descent procedures. Furthermore, confidence analysis in classical statistics is inferred from asymptotic theory assuming large datasets, which simply does not always hold in practice, e.g. (King et al., 2010). The combination of Bayesian statistics and reflectance estimation has had little attention in recent years.

In our approach, we focus on patchwise BRDF acquisition that ensures sufficient data even when not many input images are available. The estimation of pixelwise BRDF parameters requires a large amount of data to be available at every surface point to reliably fit the desired BRDF model, e.g. (Lensch et al., 2003; Goldman et al., 2005). In fact, a dense angular representation is necessary to capture narrow specular lobes and prevent aliasing. Due to shadowing effects, a complex surface structure can reduce the available intensity information per pixel to be smaller than the number of captured images. We assume isotropic reflectance and neglect the influence of subsurface scattering or translucency.

2 RELATED WORK

The scope of BRDF reproduction in previous work ranges from the acquisition of pure albedo information to the reconstruction of per-pixel sets of parameters of complex BRDF models, e.g. Weyrich et al. (2008); Aittala et al. (2013).

A common approach to estimate the SVBRDF of an unknown material is to compute mixture maps as-

Lenoch, M., Wilhelm, T. and Wöhler, C.
Simultaneous Surface Segmentation and BRDF Estimation via Bayesian Methods.
DOI: 10.5220/0005722600390048
In *Proceedings of the 11th Joint Conference on Computer Vision, Imaging and Computer Graphics Theory and Applications (VISIGRAPP 2016) - Volume 4: VISAPP*, pages 39-48
ISBN: 978-989-758-175-5
Copyright © 2016 by SCITEPRESS – Science and Technology Publications, Lda. All rights reserved

suming weighted sums of base materials to construct an approximation of the measured intensity Goldman et al. (2005); Alldrin et al. (2008); Lenoch et al. (2014). These base materials are either taken from densely acquired datasets, e.g. the MERL database Matusik et al. (2003), or composed of few analytical BRDF models. In the latter case, the set $\boldsymbol{\theta}$ of parameters of the model function has to be estimated. Goldman et al. (2005) assume two base materials per surface and represent those with a mixture of two Ward-BRDFs. Similarly, Lensch et al. (2003) capture reflectance samples that yield salient information and apply mixtures of up to five Lafortune BRDFs to clustered lumitexels. This yields more possibilities in the model space, but requires the estimation of multiple sets of parameters and a mixture map at the same time.

The combination of BRDF estimation and probabilistic methods is very rare in literature. Aittala et al. (2013) represent reflectance that may vary along the surface by a Gaussian mixture model in the frequency domain. The initial solution is improved with a maximum a-posteriori estimation. Louw and Nicolls (2010) use a Markov random field to imitate the reflectance behavior of a surface. The MRF is estimated with a Population Markov Chain Monte Carlo algorithm Laskey and Myers (2003).

3 PROPOSED PROCEDURE

The BRDF fitting procedure requires the illumination geometry to be known. This can be ensured easily, if 3D information about the surface is available. However, the approach works independent of the source of the 3D data and could be integrated in a self-consistent algorithm similar e.g. to Herbort and Wöhler (2012), that has no prior knowledge about the surface shape.

3.1 Bayesian BRDF Modeling

We choose the BRDF model according to Blinn (1977) in the physically plausible modification by Giesen (2009) combined with a Lambertian term (Lambert, 1760) to account for diffuse reflection. We assume that this relatively simple model suffices, since the unknown surface will be segmented during the procedure and complex reflectance can be modeled by small segments of different parameters. Note that we do not require physical materials to coincide with segmented patches, since even within the same material subtle changes can require changing BRDF parameters to achieve accurate modeling.

In terms of Bayesian statistics, the BRDF model is the mean of a normal distributed likelihood. We assume the residuals of the BRDF model to follow a Gaussian distribution with an unknown variance σ^2. Since σ^2 is unknown, we estimate it as a part of the procedure and are thus able to quantify the deviation of the model from the observed data which based on the BRDF model formulation by Giesen (2009) leads to

$$\boldsymbol{y} \sim \mathcal{N}(\boldsymbol{\mu}, \sigma^2) \tag{1}$$

$$\boldsymbol{\mu} = \frac{I_0}{r^2}\left(\frac{k_d}{\pi} + k_s \frac{(\gamma+2)(\gamma+4)}{8\pi(2^{-\frac{\gamma}{2}}+\gamma)} \cdot \langle \mathbf{h}\cdot\mathbf{n}\rangle^{\gamma}\right)\langle \mathbf{l}\cdot\mathbf{n}\rangle \tag{2}$$

$$1 = k_d + k_s. \tag{3}$$

Here $\langle \mathbf{l}\cdot\mathbf{n}\rangle = \cos\angle(\boldsymbol{l},\boldsymbol{n})$ denotes the vector product between the normalized vectors $\boldsymbol{l}$ and $\boldsymbol{n}$, with surface normal $\boldsymbol{n}$, direction $\boldsymbol{l}$ of incident light, viewing direction $\boldsymbol{v}$ and half-way vector $\boldsymbol{h} = \frac{\boldsymbol{l}+\boldsymbol{v}}{||\boldsymbol{l}+\boldsymbol{v}||_2}$.

The chosen model thus depends on four parameters. Light source intensity I_0, diffuse and specular weight k_d (since $k_s = 1 - k_d$), cosine lobe exponent γ and variance σ^2. Each of these parameters requires a prior to define the distribution of the parameter before any data was seen. We assume the priors to be normal distributions; exemplarily for the light source intensity

$$p(I_0) \sim \mathcal{N}(\mu_{I_0}, \sigma^2_{I_0}) \tag{4}$$

The prior yields the possibility to involve certain knowledge about the possible range of the parameters into the estimation process. This fact can be exploited if, for example, a coarse estimate of the light source intensity exists. Yet, this estimate might be prone to simplification errors. If there is no prior knowledge available or only at a high level of uncertainty, a large variance is used to reduce the influence of the prior, since its probability is equal in almost the entire parameter space. In a Bayesian framework this is termed an *uninformative prior*. A uniform distribution would cancel out the effect of the prior completely.

Concluding from Bayes' law we can now compute the probability distribution of the set $\boldsymbol{\theta}$ of model parameters for the input intensity data $\boldsymbol{Y}$ and the a-priori probability $p(\boldsymbol{\theta})$.

$$p(\boldsymbol{\theta}|\boldsymbol{Y}) = \frac{p(\boldsymbol{Y}|\boldsymbol{\theta}) \cdot p(\boldsymbol{\theta})}{p(\boldsymbol{Y})} \tag{5}$$

The normalization factor $p(\boldsymbol{Y})$ is difficult to estimate and can be omitted, since it is constant as long as the input data does not change. Therefore the posterior-density can be expressed as

$$p(\boldsymbol{\theta}|\boldsymbol{Y}) \propto p(\boldsymbol{Y}|\boldsymbol{\theta}) \cdot p(\boldsymbol{\theta}) \tag{6}$$

All information required to determine the probability distribution of the set of model parameters for

the given input data is the likelihood and the prior, which is both at hand.

3.2 Markov Chain Monte Carlo

Actually, the chosen priors can be based on additional available information or be completely uninformative, in any case the real distribution of $\boldsymbol{\theta}$ remains unknown and subject to the estimation. *Markov chain Monte Carlo* (MCMC) methods as e.g. introduced by Ntzoufras (2011) can be employed to sample the model parameters' unknown distribution. To achieve this, a Markov chain is constructed whose stationary distribution corresponds to the desired unknown distribution. Thus, after a converging time, the state of the chain can be used sample the unknown posterior.

More specifically, we use the *Metropolis-Hastings* (MH) algorithm introduced by Metropolis et al. (1953) and Hastings (1970). Accordingly, we construct a Markov chain which proposes in each step new values of the chain for the respective BRDF parameters. The likelihood of the values is assessed with the newly generated values and if the likelihood of the parameters increases they are probably accepted as a new value of the chain, if not they are probably discarded. The term *probably* refers to the acceptance probability α that is compared to a random number, such that there is a possibility to accept a new value even if the likelihood decreased and vice-versa. Similar to the priors, starting values $\boldsymbol{\theta}^{(0)}$ have to be supplied by the user and can bring in additional information.

The number T of iterations of the algorithm is taken to be fixed. A proposal distribution $p(\boldsymbol{\theta}^{(t)}|\boldsymbol{\theta}^{(t-1)})$ and the acceptance probability α are necessary for the generation process; given for I_0

$$\begin{aligned} I_0^{(0)} &\quad \text{initial value,} \\ p(I_0^{(t)}|I_0^{(t-1)}) &\sim \mathcal{N}(I_0^{(t-1)}, (\sigma_{I_0}^p)^2) \end{aligned} \tag{7}$$

$$\begin{aligned} \alpha_{I_0} &= \min(1, A) \\ A &= \frac{p(\mathbf{y}|I_0^{(t)}, k_d, \gamma, \sigma) p(I_0^{(t)}) p(k_d) p(\gamma) p(\sigma)}{p(\mathbf{y}|I_0^{(t-1)}, k_d, \gamma, \sigma) p(I_0^{(t-1)}) p(k_d) p(\gamma) p(\sigma)} \Bigg) \\ &= \min\left(1, \frac{p(\mathbf{y}|I_0^{(t)}, k_d, \gamma, \sigma) p(I_0^{(t)})}{p(\mathbf{y}|I_0^{(t-1)}, k_d, \gamma, \sigma) p(I_0^{(t-1)})}\right) \end{aligned} \tag{8}$$

It is assumed here that there is no interdependence between the parameters, such that we can apply a *componentwise* MH and each parameter is proposed and accepted individually (Ntzoufras, 2011). This yields the general advantage, that simple proposal distributions can be applied, whereas the construction of a combined proposal distribution can require careful design. Still, a combined proposal distribution can yield a faster converging chain.

After a user-defined *burn-in* phase the chain converges to the actual unknown posterior distribution if according to Gilks et al. (1996, p.46) the following properties are met:

- Irreducibility
- Positive Recurrency
- Aperiodicity

At the state of convergence, statistics can be computed from the drawn samples. Thusly, the adaption of the BRDF model to unknown data immediately yields a confidence region for each parameter and with $\boldsymbol{\sigma}^2$ a measure of the accuracy of the model.

3.3 Reversible Jump Markov Chain Monte Carlo

So far we can adapt a BRDF model to unknown intensity data, but the segmentation of the surface has not yet been regarded. Image segmentation is usually performed in a generative way (e.g. using *Gaussian Mixture Models*). We use instead a discriminative approach and directly infer the boarders of the regions from the data. Effectively, a change in surface structure or material enforces a change of the model parameters to reproduce the received impression accurately.

So-called *Reversible Jump Markov chain Monte Carlo* (RJMCMC) methods as described by Green (1995) are able to explore the parameter and model space simultaneously. That means in terms of statistics, that there is a certain probability in each iteration to create, delete or modify a *change point* τ that separates two sets of model parameters. Using these change points it is possible to divide unknown data into meaningful segments.

We have extended the concept of change points to the two-dimensional application of image segmentation, with the following new properties:

- Change points are possible both in u and v direction (referring to image coordinates).
- A change point becomes a vector of change points, since it will affect the entire row/column of image pixels.
- Each pixel coordinate of the change point vector can be moved individually.
- Surface segments are constructed from the regions where the same change points in u and v direction coincide.

We allow change points to lie outside of the image coordinate frame, since this is a helpful property when segment borders are not covering a complete row or column.

A possible maximum of change points in each direction has to be defined by the user. Based on these maxima, we construct an indicator matrix that assigns the actual regions based on the combinations of the change points. For example, $\tau_{\max}(u) = \tau_{\max}(v) = 3$ yield the following assignment:

$$\begin{bmatrix} (1,1) & (1,2) & (1,3) \\ (2,1) & (2,2) & (2,3) \\ (3,1) & (3,2) & (3,3) \end{bmatrix} \hat{=} \begin{bmatrix} 1 & 4 & 7 \\ 2 & 5 & 8 \\ 3 & 6 & 9 \end{bmatrix} \quad (9)$$

Each change point itself has a statistical distribution, such that confidence intervals can be computed directly from the data of the Markov chain. Compared to other segmentation procedures this is a noteworthy advantage, since the algorithm gives a measure for the quality of the segmentation. The change points are assumed to follow a uniform distribution, s.th. $\tau \sim \mathcal{U}(-1, \text{imagesize}+1)$, since they are allowed to lie outside the image plane

3.3.1 A Change in Dimension

The possibility to create or delete change points creates needs of a procedure to split and merge parameter sets $\boldsymbol{\theta}_i$. A new region could be initialized with the parameters of a randomly chosen neighboring region, yet this makes it impossible to revert the step without storing a large amount of data. A better solution is to have a bijective transformation $\boldsymbol{M}$ which is independent of the actual number of change points.

A random number r is drawn from the distribution $q(r) = \mathcal{N}(0,1)$ and symmetrically added and subtracted from the existing change points. Inspired by Pascal's triangle the coefficients $P_n(k) = (-1)^k \binom{n}{k}, k = 0,..,n$ of the last column of $\boldsymbol{M}$ create a unique transformation when *jumping* from dimension $n-1$ to n. For the step to $n = 3$ and former parameters $\boldsymbol{\theta}_1^{(t-1)}$ and $\boldsymbol{\theta}_2^{(t-1)}$ this means

$$\begin{bmatrix} \boldsymbol{\theta}_1^{(t)} \\ \boldsymbol{\theta}_2^{(t)} \\ \boldsymbol{\theta}_3^{(t)} \end{bmatrix} = \begin{bmatrix} 1 & 0 & -1 \\ 0.5 & 0.5 & 2 \\ 0 & 1 & -1 \end{bmatrix} \begin{bmatrix} \boldsymbol{\theta}_1^{(t-1)} \\ \boldsymbol{\theta}_2^{(t-1)} \\ r \end{bmatrix}. \quad (10)$$

Note that the transformation has to be applied componentwise to $\boldsymbol{\theta}_i$, thus the random number r can be scaled to the dimension of the parameter. The inverse of $\boldsymbol{M}$ is defined and the Markov chain can be reset to its state in the lower dimension. This can be helpful to reduce computational time, since the chain can continue from its former state, possibly near convergence.

The proposed change in dimension is accepted with an acceptance probability α similar to the proposition of new parameters. The dimension is represented by a model number m that is determined from the indicator matrix. For the sake of readability the iteration index t will be omitted in what follows and the proposed value is indicating by an apostrophe.

$$\alpha(\boldsymbol{\theta}, \boldsymbol{\theta}') = \min(1, B),$$
$$B = \frac{p(\boldsymbol{\theta}', m'|\boldsymbol{X}) p(m|m') q(r')}{p(\boldsymbol{\theta}, m|\boldsymbol{X}) p(m'|m) q(r)} \left| \frac{\partial \boldsymbol{\theta}'}{\partial(\boldsymbol{\theta}, \boldsymbol{r})} \right| \quad (11)$$

$p(m'|m) = p(m|m')$ is the probability to change from one model to the other, e.g. add or delete a change point respectively and in our approach assumed to be equal. $\left| \frac{\partial \boldsymbol{\theta}'}{\partial(\boldsymbol{\theta}, \boldsymbol{r})} \right|$ is the Jacobian of the partial derivatives, necessary since what we do is basically a coordinate transformation. Yet, the Jacobian is only a scaling factor, which may be omitted and thus B simplifies to

$$B = \frac{p(\boldsymbol{\theta}', m'|\boldsymbol{X}) q(r')}{p(\boldsymbol{\theta}, m|\boldsymbol{X}) q(r)}. \quad (12)$$

The acceptance of the inverse move is simply calculated as

$$\alpha = \min\left(1, \frac{1}{B}\right). \quad (13)$$

After the predefined number of T iterations, it has to be decided which combination of change points is the most probable. The integration in the model space is turned into a summation in the discrete case and the model with the most iterations is accepted as the best solution, e.g. (King et al., 2010). However, comparing the "time spent" in different models yields information about the certainty of the solution.

3.4 Synthetic Data

The algorithm is evaluated first on a synthetic dataset. Figure 1(a) shows one of the input images and Figure 1(b) the resulting reflectance map. The similarity to the result expected by the human viewer underlines the success of the algorithm in determining the reflectance parameters of the surface and segmenting its regions. The parameters of the algorithm, $(\sigma_i^p)^2$ of the proposal distribution, the prior parameters and the starting values of the Markov chain $\theta_i^{(0)}$ are stated in Table 1.

The histogram of visited models is depicted in Figure 2. The histogram counts indicate strongly that model $m = 8$ is the best choice. That equals one

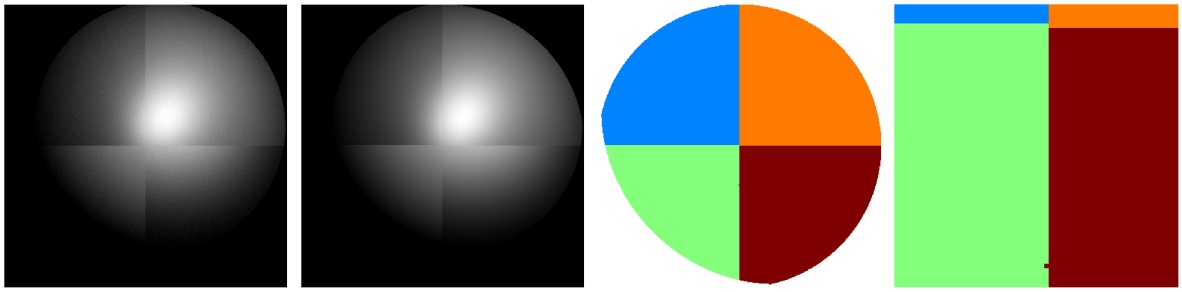

(a) (b) (c) (d)

Figure 1: (a) Exemplary input image of synthetic dataset and (b) reflectance map computed from the algorithm. Same grey value scaling in both images. (c) Assignment of regions is almost perfect. (d) Misaligned pixel in lower right region.

Table 1: Initial values $\theta_i^{(0)}$ of Markov chain, $(\sigma_i^p)^2$ of proposal distribution and prior parameters μ_{prior} and $(\sigma_{\text{prior}})^2$.

	$\theta_i^{(0)}$	$(\sigma_i^p)^2$	μ_{prior}	$(\sigma_{\text{prior}})^2$
I_0	80	0.5	0	100
k_d	0.5	0.05	0	100
γ	1	0.07	0	100
σ^2	3	0.09	0	100

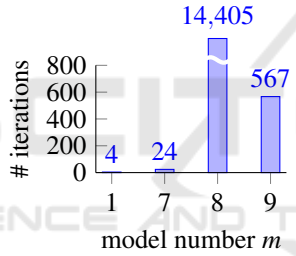

Figure 2: Histogram of visited models in model space of artifical dataset. Counting indicated that model 8 is the most likely one.

change point in u and v direction and is highly consistent with the dataset, as becomes apparent from Figure 1. The certainty of the algorithm is about 96%.

The sampled a-posteriori distribution of the set $\boldsymbol{\theta}$ of model parameters is shown along with the iterations of the Markov chain in Figure 3. Convergence of k_d and γ is slow which may be caused by the small $(\sigma_i^p)^2$ of the proposal distribution (see Table 1). To ensure that the final sampling is based on the correct a-posteriori distribution, the burn-in phase is set to 50%, which is a conservative estimation.

To underline the efficiency of our procedure, the inferred reflectance parameters and their uncertainties are listed in Table 2 together with the true values that have actually been used to generate the synthetic test data (green values in each cell). The averages of the parameter estimates are very similar to the actual parameter values, which is also indicated by Figure 1(a) and (b). Moreover, the uncertainties of the estimate

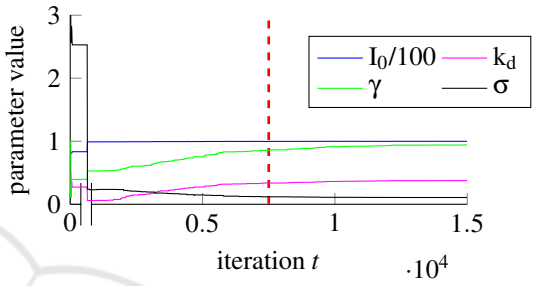

Figure 3: Change of parameters of upper region for $m = 8$ (most likely model) throughout iterations. The light source intensity has been scaled to improve visibility. I_0 and σ converge very fast to a stationary distribution, whereas k_d and γ converge slowly. This can be caused by the small values of $(\sigma_i^p)^2$ of the proposal distribution. The red dashed line indicates the end of the assumed burn-in phase after 50% of the total iterations.

are very low, such that the confidence band is a narrow tube that shows the high accuracy of the procedure on the data set.

The uncertainties of the values of the lower right region are notably higher. This might be caused by the data set itself, since the light sources are not distributed symmetrically around the sphere to create realistic conditions. Thus, the lower right region possibly yields less salient information than the remaining surface, e.g. intensity data that defines the cosine lobe. However, the synthetic data should be regarded as a *proof of concept*, and applying the method to real-world data will be a more valuable assessment.

4 APPLICATION

The proposed method is applied both to artificial and real world data. The artificial data consists of 10 images of a sphere that are rendered with the Lambert-Blinn BRDF model lighted from different positions, the surface is divided into four segments. The shading BRDF parameters of the individual patches are given

SCITEPRESS SCIENCE AND TECHNOLOGY PUBLICATIONS

Table 2: Maximum a-posteriori estimate of parameters and 1σ deviation for upper and lower region after burn-in phase of 50%. The green values have been used render the synthetic images and are therefore the target values of the optimization.

θ_i	upper left		lower left		upper right		lower right	
I_0	100.0 ± 0.001	100	100.0 ± 0.007	100	100.0 ± 0.002	100	99.87 ± 0.048	100
k_d	$0.499 \pm 4.2 \cdot 10^{-5}$	0.5	$0.899 \pm 1.3 \cdot 10^{-4}$	0.9	$0.599 \pm 6.9 \cdot 10^{-5}$	0.6	0.363 ± 0.012	0.4
γ	$4.99 \pm 9.6 \cdot 10^{-4}$	5	9.99 ± 0.015	10	$4.99 \pm 1.6 \cdot 10^{-3}$	5	0.91 ± 0.026	1
σ^2	$0.10 \pm 2.2 \cdot 10^{-4}$	0.1	$0.10 \pm 2.3 \cdot 10^{-4}$	0.1	$0.10 \pm 1.6 \cdot 10^{-4}$	0.1	0.11 ± 0.004	0.1

Table 3: Initial values $\theta_i^{(0)}$ of Markov chain, $(\sigma_i^p)^2$ of proposal distribution and prior parameters μ_{prior} and $(\sigma_{\text{prior}})^2$.

	$\theta_i^{(0)}$	$(\sigma_i^p)^2$	μ_{prior}	$(\sigma_{\text{prior}})^2$
I_0	1	0.1	1	1
k_d	0.5	0.01	0.5	1
γ	25	10	25	100
σ^2	1	0.1	0.1	100

in Table 2 (green values). Noise is added to the image data to create more realistic conditions.

The real-world dataset contains 18 HDR images of the test object. We used the measurement equipment in our laboratory[1] to acquire both image and depth data of a painted plaster object. The illumination environment is calibrated according to Lenoch et al. (2012).

4.1 Real-world Data

The test object consists of shaped plaster that has been divided into three patches of which two are painted with green and blue acrylic paint, respectively. The object was designed to be of a geometrically complex shape and yield multiple reflection characteristics at different surface areas. Due to the acquisition with a monochrome camera both painted regions appear very similar even to the human viewer. Thus, two regions can be segmented. One is bright white and exhibits diffuse reflection while the other is dark grey and shows increased specular reflection from the shiny paint. Table 3 displays the initial values of the Markov chain $\theta_i^{(0)}$, the $(\sigma_i^p)^2$ of the proposal distribution and the prior parameters.

The object is depicted in Figure 4(a). Figure 4(b) and (c) display the corresponding reflectance map based on the Lambert-Blinn BRDF model (Blinn, 1977) and the estimated parameters and segmentation as well as a pixelwise error map. For the sake of simplicity only one image of the object from the entire real-world data set is given. The largest deviations can be spotted at the dents in the upper region and at the shiny component of the lower region which is not bright enough. These findings are supported by Figure 4(c). The high difference in the dents is caused by masking and interreflection effects on the real surface that are not modeled by the BRDF. The errors in the segmentation will be addressed later.

First of all, it has to be stated that the segmentation of the surface is not intensity based, which one might consider suitable for this object, but based on the likelihood that a certain set of parameters fits the designated surface patch best. The shadowed parts of the dents might be assigned to the lower patch if it was purely intensity based. Furthermore, the glossy specular component of the lower region yields an intensity which is close to the bright areas of the upper region. This demonstrates one great advantage of the segmentation based on reflectance functions: A shiny surface is not separated based on the fact that the image intensity varies significantly from diffuse to specular component. This property is elaborated further in Section 5.

Secondly, the procedure is able to detect that a segmentation of the surface into two regions yields the best results. Figure 5 indicates that the model $m = 2$, one change point vector in u direction, was visited $T_2 = 13178$ times and thus has a probability of $\approx 87,85\%$ to be the best choice.

The estimated parameters of the two BRDFs and their 1σ uncertainties are listed in Table 4. The intensity value I_0 accounts for the changing brightness of the surface, whereas the diffuse component is almost equal. The estimated noise σ^2 of the likelihood is very small, indicating that the estimated BRDF values cover the measurements well. The cosine-lobe parameter γ shows a high uncertainty that is caused by the large diffuse component. Since $k_s = 1 - k_d \Rightarrow k_s \approx 0.04 \ldots 0.06$ the cosine lobe has very little effect on the final reflectance map. However, the larger exponent of the lower region is consistent with the impression of the shinier surface, although the specular component in the reflectance map is too small.

The progression of the Markov chain of $\boldsymbol{\theta}$ (upper region) is depicted in Figure 6. The dotted red line marks the end of the burn-in phase, after which the chain is supposed to have converged to their true dis-

[1] 3D Scanner: zSnapper Vario with AVT Pike 421-F, CCD sensor, resolution 2048x2048 pixel. Light sources: Seoul P4 Power LED, centered at a wavelength of 525 nm.

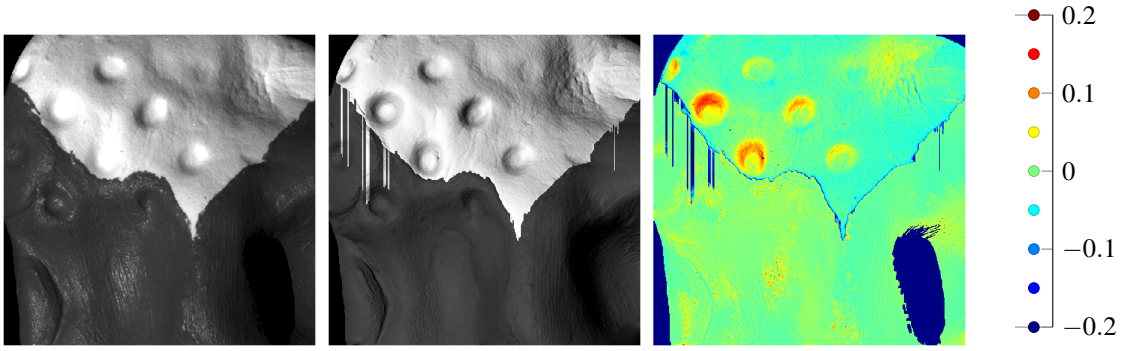

(a) (b) (c)

Figure 4: (a) One of the captured images, (b) reflectance map of segmented surface with computed parameters. Same scaling of grey values in both images. (c) Absolute difference of intensity values.

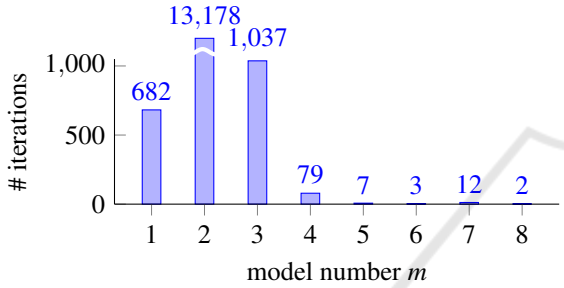

Figure 5: Histogram of visited models in model space. Counting indicated that model 2 is the most likely.

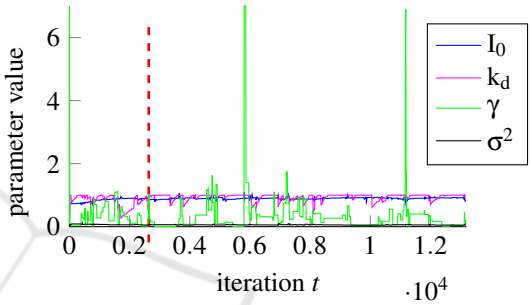

Figure 6: Change of parameters of upper region for $m = 2$ (most likely model) throughout iterations. Most parameters converge fast to an almost stationary value, γ shows a higher uncertainty, the red dashed line indicates the end of the assumed burn-in phase after 20% of the total iterations.

Table 4: Maximum a-posteriori estimate of parameters and 1σ deviation for upper and lower region after burn-in phase of 20%.

θ_i	upper Region	lower Region
I_0	0.899 ± 0.029	0.241 ± 0.004
k_d	0.939 ± 0.098	0.968 ± 0.012
γ	0.338 ± 0.747	32.65 ± 4.068
σ^2	0.056 ± 0.007	0.016 ± 0.002

tribution. It is visible here as well that all parameters except γ have converged fast to an almost stationary value, whereas γ suffers from the small specular component which makes its estimation difficult.

As already seen in Figure 4(b) the estimation of the change points yields errors at the outer parts of the object. The mode of the distribution of each change point (blue line) and the 95% confidence level (magenta dashed line) is shown in Figure 7(a). The yellow box frames the region of high certainty that coincides with the correct segmentation. The erroneous change points yield a drastically increased uncertainty and as such the algorithm itself is able to determine when to trust a change point and when not.

A closer look at the estimated change points is possible with Figure 7. The histogram of each change point is given in Figure 7(b) and it is evident that the correct segmentation has been part of the proposed change point values and more often than other values as indicated by the color. Yet, many other change points have been proposed and accepted such that the resulting confidence level is low and the mode of the distribution does not always coincide with the segmentation ground truth.

A possible cause of the reduced quality of the segmentation is the lack of data at the outer regions of the object. Figure 8 shows the number of valid images per surface pixel. It is apparent that the outer object surface yields less available information and thus increases the difficulties of finding the correct change points and BRDF parameters.

5 EVALUATION

To assess the prospects of the presented method, we compare the results of the segmentation to common image segmentation procedures. We apply k-means, e.g. (Seber, 1984; Spath, 1985), Gaussian mixture model[2] (GMM) (McLachlan and Peel, 2000),

[2]Matlab 2015a implementation of k-means and GMM.

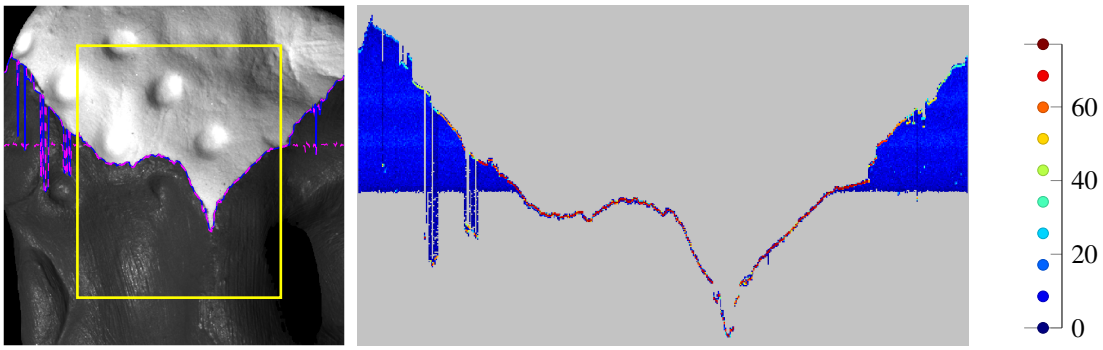

(a) (b)

Figure 7: (a) Position of change points (blue line) and 95%-confidence tube (magenta dashed line) showing the uncertainty. The part inside the yellow box is segmented at high accuracy. The outer parts of the object show erroneous segmentation in combination with an increased uncertainty. (b) 2D Histogram of change points after burn-in phase. Each column represents the histogram of the respective change point in u direction, the color indicates the histogram counts per pixel. The image has been zoomed to enlarge the area of interest and the square root has been applied to all counts to improve visibility.

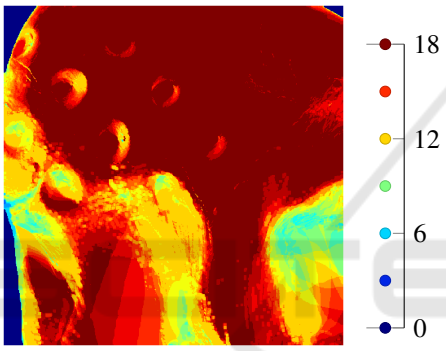

Figure 8: Valid images per pixel available to the BRDF estimation. The outer region lacks data, which is caused by shadowing or outlying illumination geometry and makes the accurate BRDF estimation more difficult.

multichannel k-means (Pichler and Hosticka, 1995) and normalized graph cuts[3] (NCuts) (Shi and Malik, 2000) segmentation procedures. The cluster algorithms are applied to the synthetic data, since the varying intensity and specular highlights are the more challenging dataset to be accurately segmented.

Note that the comparison of these algorithms to ours is questionable since the similarity criterion used to dissect the surface is not the same in every procedure. Our methods operates on the average similarity of measured grey values and a rendered image. The segmentation procedures compared against our method use grey values to dissect the image. In the case of GMM we extended the input data with spatial information about the pixel location. Furthermore, NCuts can not handle multiple input images without modification. However, to our knowledge there is no method that yields a similar approach to image segmentation as the one presented in this paper.

k-means. Multichannel image data can be exploited in a k-means clustering when treating each of the P images as a separate feature of every pixel, such that we get $N \cdot M$ samples (assuming I_{NxM}) each yielding P features. Since k-means requires that the desired number of clusters is provided by the user, we tried $k \in [48]$. The k-means segmentation of the synthetic dataset is displayed in Figure 9. The segmentation is erroneous for every considered number of clusters. Since k-means operates on grey values, the specular highlights of the surface determine the dominant center of the clusters.

The multichannel k-means algorithm as described by Pichler and Hosticka (1995) did not converge to a solution on the given data.

Gaussian Mixture Model. Similar to the k-means algorithm we supplied the multiple intensities per image pixel as features to the fitting of the GMM. Moreover, we provided the spatial position of the pixel as additional feature. The GMM is not able to dissect the surface into the correct areas of different reflectance properties as can be seen in Figure 10.

Normalized Cuts. Since the normalized cuts algorithm is not designed to handle multispectral image data only one image from the dataset (Fig 11(a)) is used to test the segmentation. To account for a background-cluster the number of clusters k is increased by one. Based on $k \in \{5,6\}$ the segmentation appears reasonable, yet the borders are not perfectly met. Increasing the number of clusters leads to false segments instead of subdividing the correct segments into smaller patches.

Note that the above mentioned segmentation procedures are superior to our method in computational

[3]We used the existing implementation provided at http://www.cis.upenn.edu/ jshi/software/, last updated January 22, 2010.

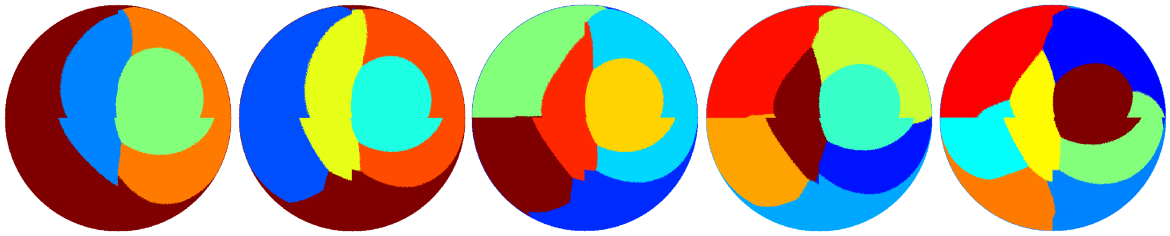

(a) $k = 4$ (b) $k = 5$ (c) $k = 6$ (d) $k = 7$ (e) $k = 8$

Figure 9: k-means segmentation of synthetic data, the colors code different surface segments. The segmentation fails for every considered setting.

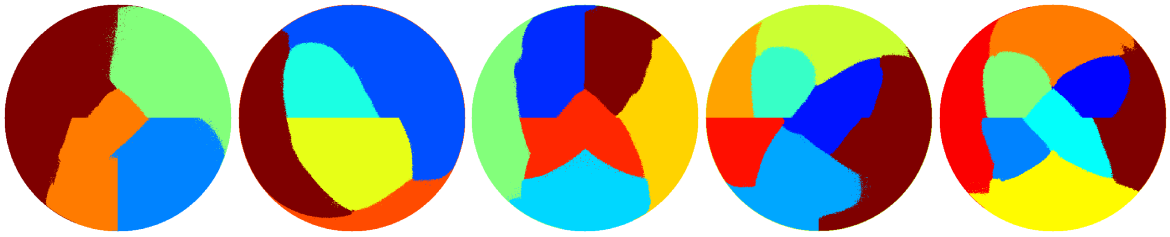

(a) $k = 4$ (b) $k = 5$ (c) $k = 6$ (d) $k = 7$ (e) $k = 8$

Figure 10: Gaussian mixture model segmentation of synthetic data, the colors code different surface segments. k is the number of Gaussian distributions fit the data. The segmentation fails for every considered setting.

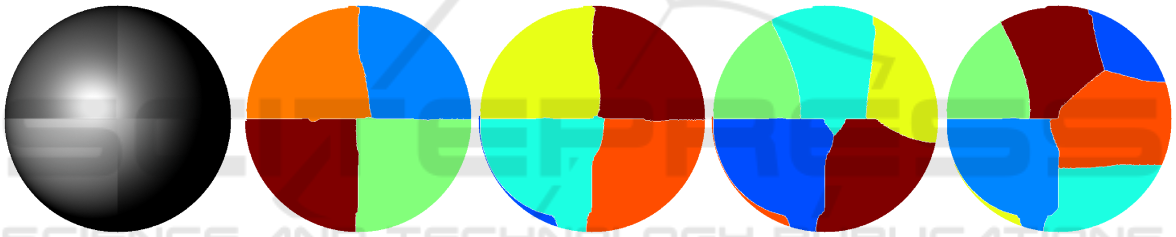

(a) (b) $k = 5$ (c) $k = 6$ (d) $k = 7$ (e) $k = 8$

Figure 11: a) Input image taken from the synthetic dataset. b)-e) Normalized cuts segmentation of synthetic data, the colors code different surface segments. The number of clusters k is increased by one with regards to the actual number of surface segments to account for a background cluster.

time. However, the general benefit of the Bayesian approach is the inherent knowledge of the uncertainty of the computed results. Furthermore, the reflectance parameters of the segmented patches need to be computed separately if e.g. used in surface reconstruction applications such as shape from shading (Horn, 1986) or photometric stereo (Woodham, 1980). Since the surface segmentation in the presented algorithm is directly based on the reflectance estimation, the parameters of the surface segments including their uncertainty are already known. Additionally, the methods used for comparison require the number of desired clusters as user input, which is not necessary in our approach since it achieves unsupervised surface segmentation.

6 CONCLUSIONS

In this paper we have shown that the segmentation of an arbitrary surface is possible based on the maximum a-posteriori estimation of its reflectance parameters. The novelty of our procedure is the direct inference of patch borders and BRDF parameters from the data and the computation based on Bayesian statistics, which inherently allows us to deduce the accuracy of the computed results. The experimental evaluation has demonstrated that the amount of available data has to be high enough to draw the correct conclusions from the input data.

In comparison to existing surface segmentation procedures our method based on the surface reflectance properties achieves the best segmentation on the synthetic dataset.

The proposal of new change points in the existing

implementation is randomized and therefore favors lines, which makes it difficult to segment circle-like surface patches, since those have to be based on lines that converge from opposing sides of the circle. Consequently, a different concept of change point proposition adapted from prior knowledge of the type of surface segments would enhance the performance of the procedure.

Furthermore, we would like to extend our method to other BRDF (likelihood) functions which consider Fresnel effects and shadowing/masking, e.g. (Cook and Torrance, 1981), or introduce a more general cosine lobe model to cope for anisotropic reflection, e.g. (Lafortune et al., 1997). Moreover, it is of great interest to include the estimation of surface normals in the likelihood, which would introduce two more parameters per pixel. This will probably increase the uncertainty of the overall likelihood considerably, but at the gain of freeing the procedure from the necessity of any prior knowledge about the surface.

REFERENCES

Aittala, M., Weyrich, T., and Lehtinen, J. (2013). Practical svbrdf capture in the frequency domain. *ACM Transactions on Graphics*, 32.

Alldrin, N., Zickler, T., and Kriegman, D. (2008). Photometric stereo with non-parametric and spatially-varying reflectance. *Conference on Computer Vision and Pattern Recognition*.

Blinn, J. F. (1977). Models of light reflection for computer synthesized pictures. *Association for Computing Machinery's Special Interest Group on Computer Graphics and Interactive Techniques*, 11(2):192–198.

Cook, R. L. and Torrance, K. E. (1981). A reflectance model for computer graphics. *Association for Computing Machinery's Special Interest Group on Computer Graphics and Interactive Techniques*, 15(3):307 – 316.

Giesen, F. (2009). Phong and blinn-phong normalization factors. *online http://www.farbrausch.de/ fg/stuff/phong.pdf*, 1:1–2.

Gilks, W., Richardson, S., and Spiegelhalter, D. (1996). *Markov Chain Monte Carlo in Practice*. Chapman & Hall.

Goldman, D. B., Curless, B., Hertzmann, A., and Seitz, S. (2005). Shape and spatially-varying brdfs from photometric stereo. *International Conference on Computer Vision*, pages 341–348.

Green, P. J. (1995). Reversible jump markov chain monte carlo computation and bayesian model determination. *Biometrika*, 82:711–732.

Hastings, W. K. (1970). Monte carlo sampling methods using markov chains and their applications. *Biometrika*, 57:97–109.

Herbort, S. and Wöhler, C. (2012). Self-consistent 3D surface reconstruction and reflectance model estimation of metallic surfaces. *International Joint Conference on Computer Vision, Imaging and Computer Graphics Theory and Applications*, pages 1–8.

Horn, B. K. P. (1986). *Robot Vision*. MIT Electrical Engineering and Computer Science.

King, R., Morgan, B. J., Gimenez, O., and Brooks, S. P. (2010). *Bayesian Analysis for Population Ecology*. CRC Press.

Lafortune, E. P. F., Foo, S.-C., Torrance, K. E., and Greenberg, D. P. (1997). Non-linear approximation of reflectance functions. *Association for Computing Machinery's Special Interest Group on Computer Graphics and Interactive Techniques*, pages 117–126.

Lambert, J.-H. (1760). *Photometria, sive de mensura et gradibus luminis, colorum et umbrae*. Vidae Eberhardi Klett.

Laskey, K. and Myers, J. (2003). Population markov chain monte carlo. *Machine Learning*, 50:175–196.

Lenoch, M., Herbort, S., Grumpe, A., and Wöhler, C. (2014). Linear unmixing in brdf reproduction and 3d shape recovery. *International Conference on Pattern Recognition*.

Lenoch, M., Herbort, S., and Wöhler, C. (2012). Robust and accurate light source calibration using a diffuse spherical calibration object. *Oldenburger 3D Tage*, 11:212–219.

Lensch, H. P. A., Kautz, J., Goesele, M., Heidrich, W., and Seidel, H.-P. (2003). Image-based reconstruction of spatial appearance and geometric detail. *ACM Transactions on Graphics*, 22(2):234–257.

Louw, M. and Nicolls, F. (2010). Surface classification via brdf parameters, using population monte carlo for mrf parameter estimation. *Proc. IASTED Int. Conf. Computer Graphics and Imaging*, 11:145–154.

Matusik, W., Pfister, H., Brand, M., and McMillan, L. (2003). A data-driven reflectance model. *ACM Transactions on Graphics*, 22(3):759–769.

McLachlan, G. and Peel, D. (2000). *Finite Mixture Models*. John Wiley & Sons, Inc.

Metropolis, N., Rosenbluth, A., Rosenbluth, M., Teller, A., and Teller, E. (1953). Equation of state calculations by fast computing machines. *Journal of Chemical Physics*, 21:1087–1092.

Ntzoufras, I. (2011). *Bayesian modeling using WinBUGS*. John Wiley & Sons.

Pichler, O. and Hosticka, A. T. B. J. (1995). A multichannel algorithm for image segmentation with iterative feedback. In *Image Processing and Its Application*.

Seber, G. A. F. (1984). *Multivariate Observations*. John Wiley & Sons, Inc.

Shi, J. and Malik, J. (2000). Normalized cuts and image segmentation. *Trans. Pattern Analysis and Machine Intelligence*, 8:888–905.

Spath, H. (1985). *Cluster Dissection and Analysis: Theory, FORTRAN Programs, Examples*. Halsted Press.

Weyrich, T., Lawrence, J., Lensch, H., Rusinkiewicz, S., and Zickler, T. (2008). Principles of appearance acquisition and representation. *Association for Computing Machinery's Special Interest Group on Computer Graphics and Interactive Techniques*, pages 1–70.

Woodham, R. J. (1980). Photometric method for determining surface orientation from multiple images. *Optical Engineering*, 19(1):139–144.